Journal of Medicinal Chemistry

Article

Fragment and Structure-Based Drug Discovery for a Class C GPCR: Discovery of the mGlu5 negative allosteric modulator HTL14242 (3-chloro-5-[6-(5-fluoropyridin-2-yl)pyrimidin-4-yl]benzonitrile)

John Christopher, Sarah J Aves, Kirstie A Bennett, Andrew S Doré, James C Errey, Ali Jazayeri, Fiona H. Marshall, Krzysztof Okrasa, Maria J Serrano-Vega, Ben Tehan, Giselle R Wiggin, and Miles Congreve

J. Med. Chem., **Just Accepted Manuscript** • DOI: 10.1021/acs.jmedchem.5b00892 • Publication Date (Web): 30 Jul 2015

ACS Publications

Journal of Medicinal Chemistry is published by the American Chemical Society. 1155 Sixteenth Street N.W., Washington, DC 20036

Fragment and Structure-Based Drug Discovery for a Class C GPCR: Discovery of the $mGlu_5$ negative allosteric modulator HTL14242 (3-chloro-5-[6-(5-fluoropyridin-2-yl)pyrimidin-4-yl]benzonitrile)

John A. Christopher, Sarah J. Aves, Kirstie A. Bennett, Andrew S. Doré, James C. Errey, Ali Jazayeri, Fiona H. Marshall, Krzysztof Okrasa, Maria J. Serrano-Vega, Benjamin G. Tehan, Giselle R. Wiggin, Miles Congreve.*

Heptares Therapeutics Ltd., BioPark, Welwyn Garden City, Hertfordshire, AL7 3AX, U.K.

Corresponding Author

*Phone: +44 (0)1707 358731. Fax: +44 (0)1707 358640. Email: john.christopher@heptares.com.

ABSTRACT

Fragment screening of a thermostabilized $mGlu_5$ receptor using a high-concentration radioligand binding assay enabled the identification of moderate affinity, high ligand efficiency (LE) pyrimidine hit **5**. Subsequent optimization using structure-based drug discovery methods led to the selection of **25**, HTL14242, as an advanced lead compound for further development. Structures of the stabilized $mGlu_5$ receptor complexed with **25** and another molecule in the series, **14**, were determined at resolutions of 2.6 Å and 3.1 Å respectively.

INTRODUCTION

Glutamate is the major excitatory neurotransmitter in the central nervous system. When released, glutamate exerts its effects through ionotropic glutamate receptors (the ligand-gated ion channels 2-amino-3-(3-hydroxy-5-methylisoxazol-4-yl)propanoic acid (AMPA) receptor, kainate receptor and *N*-methyl-D-aspartic acid (NMDA) receptor) and metabotropic glutamate (mGlu) receptors.[1] Activation of glutamatergic ion channels leads to fast glutamate transmission whilst activation of the mGlu receptors is involved in modulating the strength of synaptic transmission.

The metabotropic glutamate receptors are a family of eight G protein-coupled receptors (GPCRs) which are subdivided into three groups based on sequence homology, preferred signaling pathways and pharmacology.[2] The $mGlu_5$ receptor, predominately located post-synaptically, belongs to group I and is linked to the $G_{q/11}$ family of G proteins. The $mGlu_5$ receptor is abundantly expressed in the striatum, hippocampus, amygdala and frontal cortex.[3]

Structurally, the mGlu receptors consist of a large extracellular binding domain, the Venus flytrap (VFT) domain, linked via a cysteine-rich domain to the seven transmembrane domain (TMD) which is a feature common to all GPCRs. The VFT domain is a bi-lobed structure which contains the orthosteric (glutamate) binding site. Historical drug discovery efforts focusing on the orthosteric site typically resulted in the identification of acidic glutamate-based compounds. Generally these compounds have failed to achieve appropriate pharmacokinetic profiles, brain-penetrant characteristics and subtype selectivity.[4] Subsequently, greater success and a wider diversity of chemotypes have arisen from efforts targeting alternative binding sites (allosteric sites) within the TMD. [5-8]

Compounds binding at an allosteric site which do not activate the receptor in their own right but potentiate receptor response are termed positive allosteric modulators (PAMs). Compounds which bind to an allosteric site and act as non-competitive antagonists are termed negative allosteric modulators (NAMs). At least two allosteric sites have been identified in the transmembrane domain of the $mGlu_5$ receptor, commonly referred to as the 'MPEP site' and the 'CPPHA site' (due to initially identified compounds which bind to these regions). NAMs bind to the MPEP site whilst PAMs have been identified which bind to either the MPEP site or the CPPHA site.[9,10] We have recently published the crystal structure of the TMD of $mGlu_5$ with the NAM mavoglurant bound to the MPEP site.[11]

Dysfunctions in glutamatergic signaling have been linked to numerous disorders which could at least be partially corrected by a NAM of $mGlu_5$. NAMs of the $mGlu_5$ receptor have been, or are being tested clinically in: fragile X syndrome (FXS),[12] Parkinson's Disease levodopa-induced

dyskinesias (PD-LID),[13] anxiety,[14] gastroesophageal reflux disease (GERD),[15] neuropathic pain,[16] obsessive-compulsive disorder (OCD),[17] migraine,[18] chorea in Huntington's disease[19] and depression.[20] The most advanced trials have been in FXS where mavoglurant (**1**, Chart 1) from Novartis and basimglurant (RO4917523, **2**)[21] from Roche have completed phase III and II trials respectively, however these studies failed to show efficacy.[22] Phase II data reported by Roche on the use of basimglurant as an adjunctive in major depressive disorder shows encouraging results and strengthens the approach of targeting glutamatergic systems to develop novel antidepressants with alternative mechanisms of action for use in treatment-resistant depression.[20] Clinical development of Addex Therapeutic's NAM dipraglurant **3** is ongoing in rare dystonias and Novartis have evaluated mavoglurant in a phase II OCD trial.

Chart 1. Literature $mGlu_5$ NAMs mavoglurant **1**, basimgluant **2**, dipraglurant **3** and GRN-529 **4**.

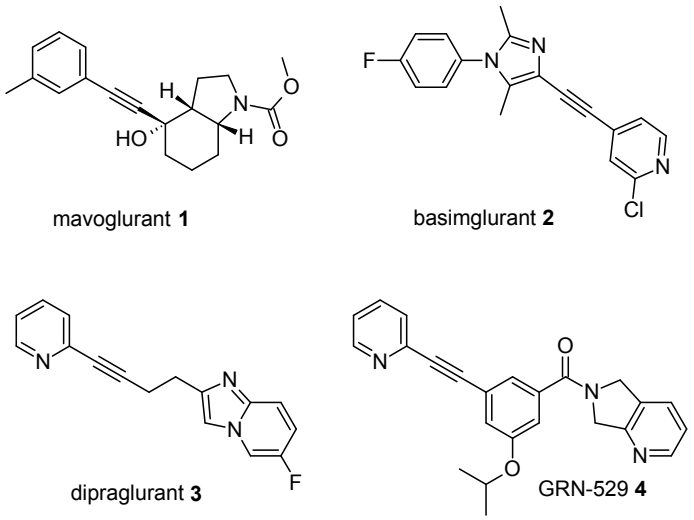

Mavoglurant, basimglurant, dipraglurant, and GRN-529 (Chart 1) are all examples of $mGlu_5$ NAM compounds containing a central acetylene flanked by two aromatic or non-aromatic

groups. The acetylene moiety has the potential to be susceptible to metabolic activation.[23] A report from Pfizer demonstrates extensive glutathione conjugation occurring at the acetylene of GRN-529 **4** (Chart 1),[24,25] implicating this as a structural link to hepatotoxicity observed in 8-week rat and non-human primate regulatory toxicology studies.[26] Workers at Bristol-Myers Squibb have reported the formation of glutathione adducts in a series of biheteroaryl acetylene $mGlu_5$ PAMs.[27] A subsequent investigation of the relationship of acetylene reactivity to the structure of the adjacent aryl groups concluded that GSH conjugation could be de-risked by flanking the triple bond with only one electron-withdrawing aryl ring. Clinical development of raseglurant, an earlier acetylene molecule from Addex, was halted in 2009 after raised alanine transaminase (ALT) levels, which are considered to be predictive of the potential for drug induced liver injury, were observed in a migraine prophylaxis trial.[28] Taken together, these reports indicate that whilst the inherent bioactivation risk residing in the acetylene can be managed, an opportunity to identify and progress non-acetylene compounds as $mGlu_5$ NAMs is evident. For the above reasons, recent efforts in the $mGlu_5$ NAM arena have focused on a second generation of non-acetylene compounds which lack the bioactivation risk.[6,7] Herein we report our own efforts to identify and characterize a novel, non-acetylene, negative allosteric modulator of the $mGlu_5$ receptor, identified through fragment screening.

RESULTS AND DISCUSSION

Fragment Screen

Within the past decade there has been a dramatic upsurge in the number of published GPCR X-ray structures,[29] which has ushered in a new era of structure-based drug discovery (SBDD) for

this highly important protein family. In tandem with SBDD, fragment-based drug discovery (FBDD) represents a powerful strategy for the identification of small, efficient molecules, and has become well established in soluble protein classes such as proteases and kinases.[30-32] We have previously reported the discovery of high affinity leads for the β_1-adrenergic receptor (β_1-AR) using structure-based and fragment-based techniques.[33] As there is ample precedent for $mGlu_5$ to be modulated by low-molecular weight ligands[6,7] we felt that the target was ideally positioned for a fragment screening approach to identify hit material. In contrast to β_1-AR, where our approach used surface-plasmon resonance (SPR) as the primary fragment screen, we opted to use a high-concentration radioligand binding assay with a stabilized receptor (StaR® protein) for $mGlu_5$ hit discovery. During the course of stabilization of the receptor to enable X-ray crystallographic studies, an intermediate $mGlu_5$ StaR protein was generated with three residues mutated from the wild-type sequence. The mutations thermostabilized the receptor, significantly increased expression over wild-type protein, and in common with other StaR proteins we have used for fragment-screening, conferred an enhanced tolerance of high DMSO concentrations. Additionally, as the thermostabilization was undertaken in the presence of the NAM radioligand [^{3}H]-M-MPEP (2-[(3-methoxyphenyl)ethynyl]-6-methylpyridine),[34] the receptor was biased into the physiologically relevant conformational state for our hit discovery campaign.[11] A final assay concentration of 10% DMSO was viable with the $mGlu_5$ StaR, facilitating screening of ligands at high concentration whilst ensuring they remained in solution. A set of approximately 3,600 fragments (including a proportion which had been selected specifically for our Class C fragment hit discovery efforts) was screened at 30 μM and 300 μM concentrations in radioligand binding format using [^{3}H]-M-MPEP in HEK293 cell membranes expressing the $mGlu_5$ StaR protein. No acetylene containing molecules were present in the screening set. Subsequently, 178 active

fragments were screened in 8-point concentration-response curves to define equilibrium dissociation constant (pK_i) values. A number of promising fragment hits emerged from the hit discovery campaign, including the ligand-efficient,[35] moderate affinity, pyrimidine **5** (Chart 2, pK_i 5.6, LE 0.36), the progression of which to an advanced lead molecule is the subject of this manuscript.

Chart 2. $mGlu_5$ fragment screening hit **5**.

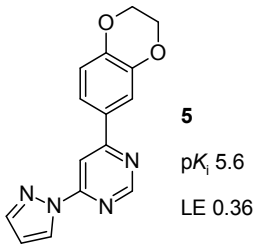

Design and Synthesis

The binding mode of **5** and analogues was initially derived from docking into an experimentally enhanced homology model of $mGlu_5$, refined using literature site directed mutagenesis information and our own extensive data set derived from receptor stabilization experiments. During the course of the project, a number of literature compounds, including mavoglurant **1**,[11] and compounds within our own series (see below), were successfully co-crystallized in the receptor which further assisted our efforts. Our initial synthetic strategy for fragment validation centered on a detailed evaluation of literature $mGlu_5$ chemotypes to identify common motifs within high affinity molecules. Hybridization of these motifs with **5** yielded compounds which were examined *in-silico* in the context of the $mGlu_5$ homology model, with molecules for synthesis selected by medicinal and computational chemists after consideration of their proposed

binding modes (Tables 1 and 2). One such motif is 3-fluoro-5-cyanophenyl, which features in several high affinity $mGlu_5$ NAM acetylene and non-acetylene chemotypes from a number of different companies, and as such was a good candidate for hybridization with **5**. Analogues of **5** were prepared using the routes summarized in Schemes 1 and 2.[36] Intermediates **18** (Scheme 1) were either commercially available or were readily synthesized from 4,6-dichloropyrimidine under mild S_NAr conditions, subsequent Suzuki-Miyaura coupling led to **6-14** and **17**. Compounds **15** and **16** were analogously accessed from the commercially available halopyridines **19** and **20**. Scheme 2 describes the routes employed to variants which replace the pyrazole by pyridines or diazines (Table 2). Pyridines **21**-**28** and pyridazine **29** employed successive palladium-mediated Stille and Suzuki-Miyaura couplings (or the reverse sequence) to yield final compounds, with the aryl stannane being synthesized from the bromo-precursor if unavailable from commercial suppliers. For **25** replacement of the Stille protocol by a nickel-mediated Negisihi coupling was additionally used, which removed the use of stoichiometric tin in the reaction sequence. Bis-pyrimidine **30** was synthesized *via* formation of a *β*-keto ester, followed by pyrimidine ring synthesis with formamidine and palladium-catalysed arylation.

Scheme 1. Synthesis of **6-17**.[a]

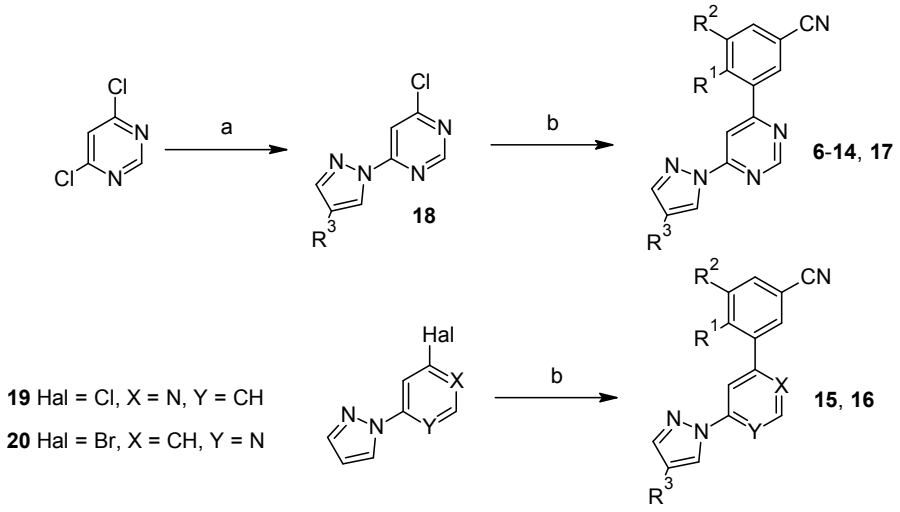

[a] Reagents and conditions: (a) Pyrazole or 4-fluoropyrazole, K_2CO_3, DMF, rt; (b) Substituted aryl boronic acid or ester, $PdCl_2$(dppf), Cs_2CO_3 or 1M(aq) Na_2CO_3, 1,4-dioxane / H_2O, 80-90ºC.

Scheme 2. Synthesis of **21-30**.[a]

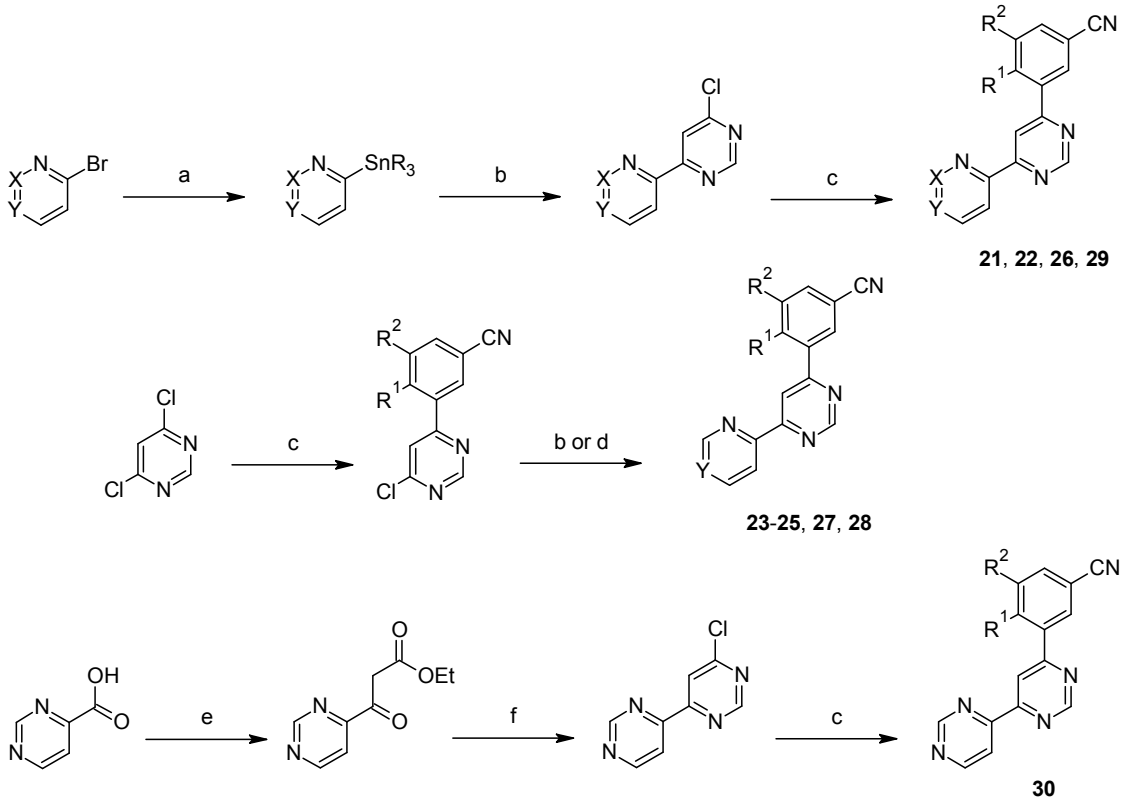

[a] Reagents and conditions: (a) R_3SnSnR_3 (R = Me or *n*-Bu), $Pd(PPh_3)_4$, DME, 80-110ºC; (b) Heteroaryl halide or stannane, $Pd(PPh_3)_4$, CuI, PhMe, 110ºC; (c) Substituted aryl boronic acid or ester, $PdCl_2(dppf)•CH_2Cl_2$, Cs_2CO_3 or 1M(aq) Na_2CO_3, 1,4-dioxane, H_2O, 80-90ºC; (d) (i) 2-Bromo-5-fluoropyridine, *i*-PrMgCl, $ZnCl_2$, THF, rt, (ii) Substituted chloropyrimidine, $Pd(PPh_3)_4$, THF, 50-60ºC; (e) (i) Oxalyl chloride, DMF, 0ºC, (ii) EtOAc, LDA, THF, -78ºC; (f) (i) $H_2NCH=NH•HCl$, NaOMe, MeOH, rt, (ii) $POCl_3$, rt.

Structure Determination of $mGlu_5$ in complex with 14 and 25

To determine the structure of the $mGlu_5$ TMD in complex with the allosteric modulators **14** and **25** a thermostabilized receptor (StaR) was generated. The receptor was thermostabilized in the presence of the allosteric radioligand [^{3}H]-M-MPEP and contained six mutations, none of which are located in close proximity to the allosteric site.[11] To further aid crystallization in lipidic cubic phase (LCP), the extracellular domains were removed from the N-terminus (residues 2-568), the

unstructured C-terminus was truncated (residues 833-1153) and finally T4-lysozyme (T4L) inserted into intracellular loop (ICL) 2 between Lys678 and Lys679. The structure of $mGlu_5$ TMD bound to **14** and **25** was determined to 3.1 and 2.6 Å respectively, through merging diffraction data from multiple crystals grown in lipidic cubic phase (LCP). The structures were solved by molecular replacement using PDB ID: 4OO9.[11] Details of data collection and refinement statistics for both structures are given in Supporting Information Table 3, in both cases the R_{free} set was imported from structure factor data deposited with PDB ID: 4OO9.

Strong and unambiguous electron density was observed for both **14** and **25** in sigma-A weighted $2m|F_o|-|DF_c|$, $m|F_o|-D|F_c|$ maps calculated using *Phenix*[37] following molecular replacement using the program *Phaser*[38] from the CCP4 suite of programs[39] (Figure 1). In general the protein backbone of the two novel structures are in close agreement with the mavoglurant co-structure with Cα r.m.s.d values of 0.23 Å and 0.26 Å between 4OO9 and the **14** and **25** structures respectively. In both the $mGlu_5$ **14** and **25** co-structures the ligands are found in the allosteric pocket (comprised of an upper and lower chamber connected by a narrow linker region) ~8 Å from the receptor surface and in a similar position to that observed previously for mavoglurant.[11] Both **14** and **25** are oriented with an approximate 30 ° tilt (relative to the central axis of the TM bundle) in a pocket defined by residues from TM2, TM3, TM5, TM6 and TM7. The pyrazole and pyridyl ring systems of **14** and **25** respectively sit in a pocket between Ala810$^{7.40}$ (superscripts indicate Ballesteros−Weinstein nomenclature[40]) and Pro655$^{3.40}$, bordered on one side by Ile625$^{2.46}$, Gly628$^{2.49}$, Ser654$^{3.39}$, Ser658$^{3.43}$ and on the other by Tyr659$^{3.44}$ and Ser809$^{7.39}$ which makes a hydrogen bond to the nitrogen within the respective pyrazole and pyridyl ring

systems (Figure 1). A number of these molecular interactions have recently been predicted in modelling studies.[41]

Both pyrazole and pyridyl ring systems are connected to a pyrimidine linker which traverses the narrow channel in the allosteric pocket formed between Tyr659$^{3.44}$, Ser809$^{7.39}$, Val806$^{7.36}$ and Pro655$^{3.40}$. In comparison to the $mGlu_5$ mavoglurant co-structure where the acetylene group of the small molecule is found crossing the linker region, here the sidechain of Val806$^{7.36}$ is shifted outwards from the binding site by ~1 Å, sterically permitting the pyrimidines to traverse the narrow channel.

The upper chamber of the allosteric pocket for the two novel structures presented here differs most significantly from that previously determined for $mGlu_5$ in complex with mavoglurant. TM6 of $mGlu_5$ contains the highly conserved Trp785$^{6.50}$ equivalent of the central toggle switch within the FxxCWxP$^{6.50A}$ motif in rhodopsin and other class A receptors. In complex with mavoglurant Trp785$^{6.50}$ is found rotated out of the helical bundle towards TM5 with a potential bifurcated hydrogen bond formed from the main-chain carbonyl of Leu744$^{5.44}$ to Gly748$^{5.48}$ to the NH of the indole ring. In both the **14** and **25** co-structures however the side-chain of Trp785$^{6.50}$ is found in a χ1 trans orientation placing the indole ring system towards the centre of the helical bundle where the NH of the indole moiety forms a hydrogen bond with Ser809$^{7.39}$. This rotameric change drastically alters the shape of the allosteric site resulting in a much smaller pocket defined primarily by Trp785$^{6.50}$, to the bottom, and Phe788$^{6.53}$ & Met802$^{7.32}$, to the top, with Ser805$^{7.35}$, Val806$^{7.36}$ & Leu744$^{5.44}$ forming the sides. The observed rearrangement of residues within the allosteric pocket would occlude binding of mavoglurant where the side-chain

of Trp785$^{6.50}$ would severely clash with the previously observed position of the saturated bicyclic ring system. The overall properties of the upper chamber of the $mGlu_5$ allosteric pocket, whilst remaining mostly hydrophobic in nature, now exhibit a greater proportion of aromatic character fitting with the SAR of the series (detailed below) and highlight the significance of utilizing a top ring system with the correct electronic character. In the case of **14** the 2-fluoro-3-chloro-5-cyanophenyl ring system is able to make complementary electronic interactions and additionally the 5-cyano substituent makes a water mediated hydrogen bond with the backbone carbonyl of Val740$^{5.40}$. In a similar fashion the 3-chloro-5-cyanophenyl group of **25** is also able to make complementary electronic interactions within the pocket and the water mediated hydrogen bond to Val740$^{5.40}$.

Whilst the allosteric pockets of the novel structures described here differ significantly in shape to $mGlu_5$ with mavoglurant bound, the crystallographic water present in the lower chamber of the allosteric pocket bridging between Thr781$^{6.46}$, Tyr659$^{3.44}$ and the backbone carbonyl oxygen of Ser809$^{7.39}$ is still observed. The water molecule is adjacent to a region where it has been proposed that observed changes in ligand pharmacology result from perturbation of the network around the water, pointing to a potential activation switch holding TM7, TM3 and TM6 together at the base of the allosteric pocket.[11] Such mode switching effects have been observed in a range of chemotypes,[42-47] but as detailed below in our series this phenomenon has not been observed in the compounds evaluated for their functional pharmacology.

Figure 1. The $mGlu_5$-StaR crystal structures with 14 and 25 bound in the allosteric site. A, Diagram of ligand interactions within the allosteric site of $mGlu_5$ with **14** bound. **B**, Diagram of ligand interactions within the allosteric site of $mGlu_5$ with **25** bound. $mGlu_5$ in ribbon representation coloured green. **14** and **25** in stick representation with carbon, nitrogen, oxygen, chlorine and fluorine atoms oxygen atoms coloured magenta, blue, red, green and white respectively. Selected residues from $mGlu_5$ in stick representation with carbon, nitrogen and oxygen atoms coloured grey, blue and red, respectively. TM helices are labeled and selected hydrogen bonds depicted as dashed red lines with distances labelled in Å. In both figures the extracellular portion of TM7 has been removed for clarity. F_o-F_c OMIT density for both ligands contoured at 2.0σ calculated prior to inclusion of the small molecule in the model. **C**, **D**, 2D diagrams of **14** and **25** ligand interactions in the $mGlu_5$-StaR allosteric pocket respectively. Green lines denote π-stack interactions, dashed purple arrows denotes hydrogen bond (side chain), solid purple arrows denote hydrogen bond (main chain), residues in cyan spheres denote polar interactions, residues in green spheres denote hydrophobic interactions.

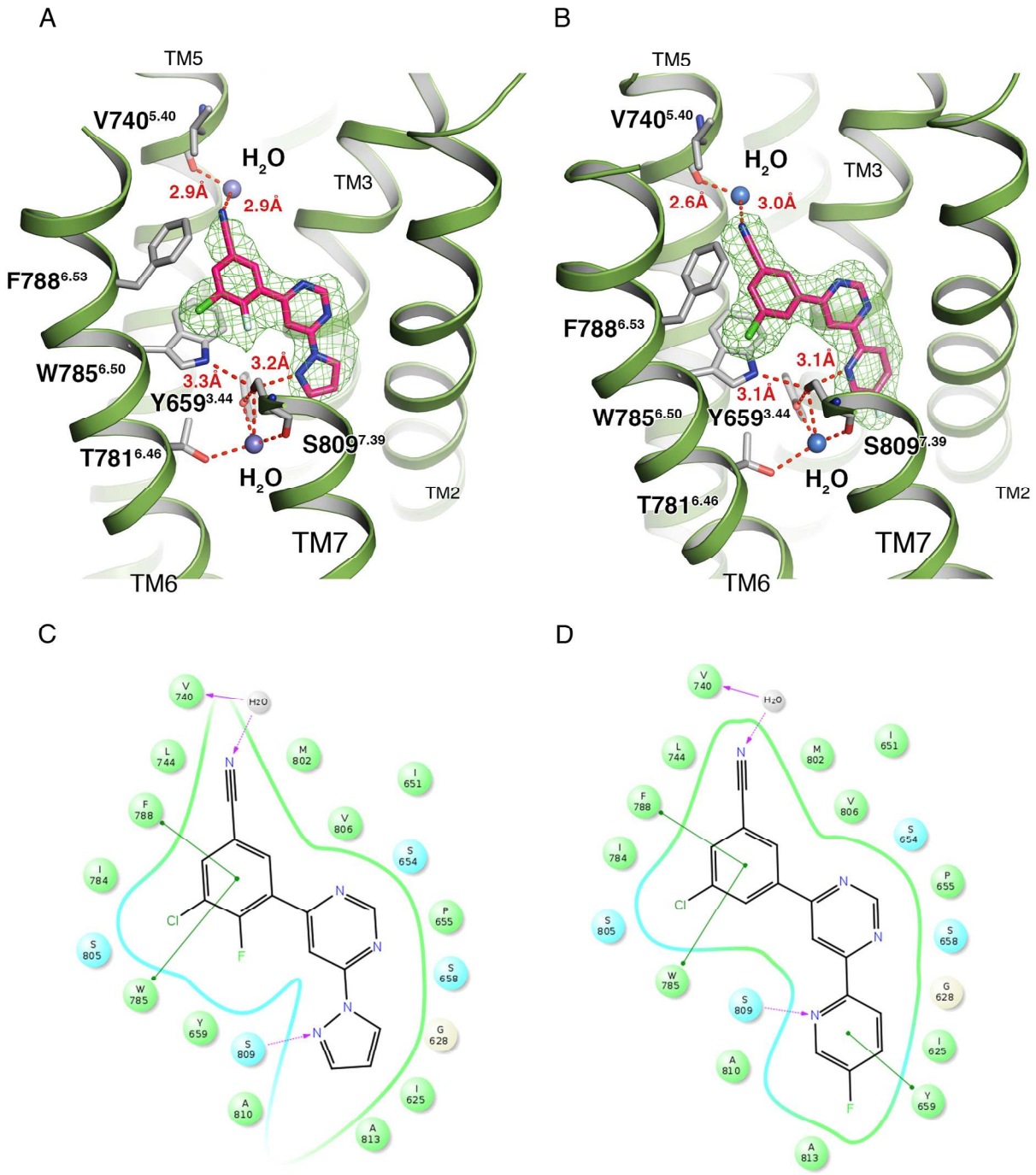
A
TM5
V740^5.40
H2O
2.9Å
2.9Å
TM3
F788^6.53
W785^6.50
3.3Å
3.2Å
Y659^3.44
T781^6.46
S809^7.39
H2O
TM2
TM7
TM6
B
TM5
V740^5.40
H2O
2.6Å
3.0Å
TM3
F788^6.53
3.1Å
3.1Å
W785^6.50
Y659^3.44
S809^7.39
T781^6.46
H2O
TM2
TM7
TM6
C
D

Structure-Activity Relationships

When tested in the $mGlu_5$ StaR fragment screening format described above, compound **6** (Table 1), which incorporated a 3-fluoro-5-cyanophenyl motif, yielded higher affinity than the initial hit (pK_i 5.6 and 6.9 for **5** and **6** respectively) and was also significantly more ligand efficient (LE 0.36 and 0.47 for **5** and **6** respectively). In a radioligand binding assay under standard conditions (1% DMSO final assay concentration, wild-type human $mGlu_5$) **6** had comparable affinity (pK_i 7.2, Table 1) as did a small number of other molecules profiled in both assay formats, allowing use of the wild-type screening assay for the remainder of the drug discovery campaign. Compounds with affinities over pK_i 7 were additionally screened in an IPone accumulation functional assay, which was configured to assess the potency (pIC_{50}) of compounds in antagonizing an EC_{80} concentration of the group 1 selective agonist L-quisqualate. In general, SAR trends in the binding assay were highly comparable to those in the functional assay. As detailed above, whilst others have reported that subtle changes to compound structure can cause mode-switching no evidence of this behavior was observed in compounds in our series which were progressed to the functional assay. The presence and position of the fluorine substituent in these analogues had a significant impact on binding affinity, with alternative regiochemistries (including **7**), or removal (**8**) of the substituent, leading to a drop in affinity. Presence of the nitrile moiety was also crucial, as removal, replacement, or hydrolysis to the primary amide of this group led to significant drops in affinity (**9**-**11**). These findings indicate that the water mediated hydrogen bonding contact with $Val740^{5.40}$ noted above is an important contributor to activity, along with the electronics of the aromatic ring structure. Keeping the nitrile in place whilst replacing the 3-fluoro substituent was encouraging, as switching fluoro to methyl (**12**) or chloro (**13**) gave approximately ten-fold increases in binding affinity, and in the latter case a

further ten-fold increase could also be gained by installing an additional 2-fluoro substituent (**14**). Investigation of the pyrimidine core of the molecule indicated that replacement by selected pyridine regiochemistries was viable with a moderate loss of binding affinity (compare **15** and **16** with **12**), whilst other pyridine or pyrimidine regioisomers and replacement by pyrazine or pyridazine resulted in significant drops in affinity, as did substitution of the ring at either of the available positions (data not shown). This SAR is consistent with the constrained nature of the allosteric pocket in the region of the narrow linker channel occupied by the pyrimidine, and also indicate that appropriately matching the electronic characteristics of the binding site in this region is important. Tight SAR was also apparent in the region of the pyrazole, efforts to substitute the ring led at best to compounds such as **17** with a moderate drop in affinity compared to the parent molecule, no substituents examined were beneficial for affinity.

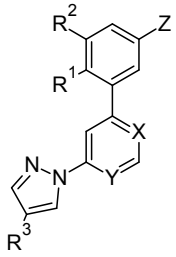

Table 1. *In vitro* profile of compounds **6-17**.

	X	Y	Z	R^1	R^2	R^3	$mGlu_5$ pK_i	$mGlu_5$ pIC_{50}	RLM $t_{1/2}$ (min)
6	N	N	CN	H	F	H	7.2	6.4	25
7	N	N	CN	F	H	H	6.6	*nd* [a]	6
8	N	N	CN	H	H	H	6.1	*nd*	*nd*
9	N	N	H	H	F	H	5.1	*nd*	*nd*
10	N	N	OMe	H	F	H	< 4.2	*nd*	*nd*

11	N	N	$CONH_2$	H	F	H	< 4.2	*nd*	*nd*
12	N	N	CN	H	Me	H	8.4	7.9	10
13	N	N	CN	H	Cl	H	8.4	8.3	12
14	N	N	CN	F	Cl	H	9.3	8.6	20
15	N	CH	CN	H	Me	H	7.6	7.4	51
16	CH	N	CN	H	Me	H	7.7	7.7	43
17	N	N	CN	H	Cl	F	7.7	7.1	52

[a] *nd* = not determined.

Despite these steric constraints, insights from the structure of $mGlu_5$ bound to **14** suggested that replacement of the pyrazole ring by alternative heterocycles was viable. A focused investigation was undertaken, which identified that 2-pyridines and certain diazines were viable replacements, whereas a number of other heterocycles were not beneficial. Compounds were synthesized using the routes depicted in Scheme 2, and SAR is summarized in Table 2. Installation of a 2-pyridyl group yielded compounds with comparable affinities and potencies to the analogous pyrazoles (compare **21** and **22** with **13** and **14** respectively). Substitution at the 4-position of the pyridine ring was tolerated with fluoro (**25**) and cyano (**26**) substituents yielding an increase in affinity and potency over the parent compound **21**; methyl (**23**) and chloro (**27**) substituents were essentially equipotent. Installation of the extra fluorine in the top aromatic ring did not significantly impact upon affinity or potency (compare **28** to **25**) but did appear to enhance *in vitro* microsomal stability (discussed further below), and the 3,5-dicyano compound **24** was also tolerated. Pyridazine **29** and pyrimidine **30** retained good $mGlu_5$ affinity, but in comparison to pyridine **21** their functional potencies dropped significantly. Other pyridine regiochemistries

were poorly tolerated, and taken together these findings highlight the importance of the hydrogen bond between Ser809$^{7.39}$ and the lower ring system.

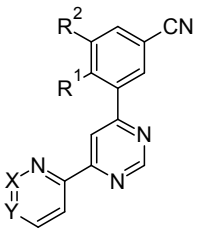

Table 2. *In vitro* profile of compounds **21-30**.

	X	Y	R^1	R^2	$mGlu_5$ pK_i	$mGlu_5$ pIC_{50}	RLM $t_{1/2}$ (min)
21	CH	CH	H	Cl	8.5	8.6	43
22	CH	CH	F	Cl	8.9	8.8	31
23	CH	CMe	H	Cl	8.6	8.3	19
24	CH	CF	H	CN	8.8	8.6	> 100
25	CH	CF	H	Cl	9.3	9.2	44
26	CH	CCN	H	Cl	9.2	9.2	> 100
27	CH	CCl	H	Cl	8.8	8.5	35
28	CH	CF	F	Cl	9.1	9.4	87
29	N	CH	H	Cl	8.0	6.7	*nd* [a]
30	CH	N	H	Cl	8.3	7.5	*nd*

[a] *nd* = not determined.

Pharmacokinetics, Receptor Occupancy and *In Vivo* Efficacy studies

As part of our routine *in vitro* profiling, we monitored stability in rat liver microsomes (RLM, Tables 1 and 2). Across a number of examples it was observed that pyridyl variants of the series

typically had better *in vitro* stability in this system, for example compare **21**, **25-28** with **13**. To examine the relationship of rat microsomal stability to *in vivo* PK parameters, we examined a number of compounds in rat iv experiments, summarized in Table 3. In general, compounds with moderate to high *in vitro* stability had moderate to high *in vivo* stability, and a small number of compounds examined with low microsomal stability also exhibited low *in vivo* stability (for example **12**, RLM $t_{1/2}$ 10 min, Cl 70 mL/min/kg), allowing us to use the RLM experiment as a filter to PK progression with a reasonable degree of confidence. Metabolite identification studies on **12** revealed a rapidly appearing single major metabolite, which was identified as the product of oxidation of the aromatic methyl group. The information allowed us to bias subsequent compound design towards molecules with less metabolically vulnerable aromatic substituents. Compounds in the series typically exhibited high brain:plasma ratios, with low, but appreciable, unbound fractions in the CNS (approximated as the ratio of drug concentration in the cerebrospinal fluid (CSF) to that in brain at the same time point).[48] Selected compounds with good rat iv PK parameters and appropriate overall *in vitro* profiles were further evaluated in dog iv/po PK studies (Table 4). Compound **25** presented the best dog profile, with moderate clearance, volume and half-life and excellent oral bioavailability, matching a similarly encouraging oral profile in rat (**25**: rat F_{po} approximately 100%, po $t_{1/2}$ 4.0 h). Rat ascending dose oral studies additionally indicated that the compound had approximately linear PK at 3, 10 and 30 mg/kg. In rat, the PK parameters of **25** compare favourably to those of key clinical standards such as dipraglurant (F_{po} 48%, po $t_{1/2}$ 1.1 h)[49] and mavoglurant (F_{po} 32%, po $t_{1/2}$ 2.9 h).[50]

Table 3. Rat intravenous PK profiles of compounds **12**, **21**, **24**-**26**.[a]

	Cl (mL/min/kg)	V_{ss} (L/kg)	$t_{1/2}$ (h)	Br : Pl (0.5, 2.0 h)		CSF : Pl (0.5, 2 h)	
12	79	2.5	0.9	1.7	1.9	0.02	0.01
21	32	4.4	2.4	1.7	1.9	0.01	*BQL*[b]
24	25	3.3	1.9	5.5	8.2	0.04	0.07
25	27	3.7	2.3	2.9	2.7	0.01	*BQL*
26	5	4.9	15.1	4.7	6.7	0.01	*BQL*

[a] Dosed at 0.5 mg/kg in rat, using 10% DMA + 10% Solutol HS15 + 80% Saline (**12**, **21**, **25**, **26**) or 10% DMA + 10% Solutol HS15 + 80% (30% (2-hydroxypropyl)-β-cyclodextrin) in saline) (**24**) as vehicle. [b] *BQL* = Below quantifiable limit of 1.00 ng/mL.

Table 4. Beagle intravenous & oral PK profiles of compounds **21**, **24**, **25**.[a]

	iv			po			
	Dose (mg/kg)	Cl (mL/min/kg)	V_{ss} (L/kg)	Dose (mg/kg)	$t_{1/2}$ (h)	AUC_{inf} (ng/h/mL)	F %
21	1[a]	36	3.9	1[a]	0.2	6	1
24	1[a]	29	5.2	5[a]	6.3	423	14
25	1[b]	27	4.9	8[c]	6.5	3946	80

[a] Dosed using 10% DMA + 5% Solutol HS15 + 85% (10% aqueous VE-TPGS) as vehicle. [b] Dosed using 10% DMA + 10% Solutol HS15 + 80% saline as vehicle. [c] Dosed using 10% DMA + 10% Solutol HS15 + 80% (10% aqueous (2-hydroxypropyl)-β-cyclodextrin).

Based on the studies detailed above and a consideration of the overall *in vitro* profile, compound **25** was selected for extensive further evaluation as summarized below and in Table 5. In common with other members of the series, the high $mGlu_5$ affinity of **25** was matched by high potency in the functional assay. In comparison, mavoglurant (pK_i 8.0, pIC_{50} 8.0) and dipraglurant (pK_i 6.9, pIC_{50} 6.9), key clinical molecules, had approximately 10-100 fold lower affinities and

potencies. In P450 inhibition assays **25** was a moderate inhibitor of 1A2 but clean against other isoforms and in P450 stability assays **25** demonstrated a balanced profile with metabolic contributions from all isoforms examined.

Moderate permeability in a Caco-2 monolayer system was observed without efflux, and in a rat brain homogenate equilibrium dialysis assay **25** demonstrated approximately 1% fraction unbound,[48] findings in line with the observed rat PK profile. The compound was stable in rat plasma, inactive at the hERG ion-channel, and had a clean profile in *in vitro* assays of cytotoxicity in HepG2 cells, and in GreenScreen cytotoxicity / genotoxicity assays in the presence and absence of S9 fractions.[51] Plasma protein binding in human and dog was high, but lower in rat. **25** was cross-screened in an external panel of 30 GPCR, kinase, ion-channel and transporter targets, where the compound displayed at least 1,000 fold selectivity against the panel members (see Supporting Information). To understand the selectivity against other metabotropic glutamate receptors, **25** was profiled in agonist, positive allosteric modulator (PAM), and antagonist/NAM modes against all eight mGlu receptors in an external screen (see Supporting Information). **25** displayed an excellent selectivity profile, with no appreciable receptor activation in agonist or PAM modes against any of the mGlu receptors. Similarly, no appreciable inhibition was observed for $mGlu_{1,2,4,6\text{-}8}$ in antagonist/NAM mode, with activity at the $mGlu_5$ receptor (97% inhibition at 10 μM) confirming our in-house characterization of the molecule. A small degree of $mGlu_3$ inhibition was noted (47% inhibition at 10 μM), though dose-response experiments were not performed to clarify the degree of selectivity against this receptor. The excellent selectivity profile across the mGlu family was not an unexpected finding, as a number of other $mGlu_5$ NAM chemotypes have been reported to have similar profiles.[52-54] Selectivity of

mavoglurant against $mGlu_1$, the other Group I metabotropic glutamate receptor and hence historically the most challenging selectivity target for orthosteric $mGlu_5$ ligands, has been reported and rationalized by comparison of the X-ray structures of the two receptors.[4,50]

Table 5. Profile of **25**, HTL14242.

$mGlu_5$ pK_i 9.3, pIC_{50} 9.2	Clean in HepG2 cytotoxicity assay, TC_{50} > 90 µM[d]
P450 pIC_{50}: 3A4/2C19/2D6/2C8/2C9 < 4.8, 1A2 5.9	Rat $f_{u,brain}$ = 1%[e]
hERG pIC_{50} < 5.5	Negative in cytotoxicity and genotoxicity screen,[f] with and without S9 fractions
Permeability[a] $13x10^{-6}$ cm s^{-1} (efflux ratio 1.0)	*Ex-vivo* binding: ED_{50} 0.3 mg/kg po
PPB%[b] >98, >98, 83	*In vivo* efficacy (mouse marble burying) ED_{50} 8 mg/kg po
Rat plasma stability 96%[c]	7-day non-GLP repeat rat toxicity – well tolerated up to 30 mg/kg/day po

[a] Caco-2 monolayer, P_{app} A-B. [b] Binding to human, canine and rat plasma proteins respectively. [c] Percent compound remaining after 60 min incubation with rat plasma. [d] Concentration causing a 50% reduction in cell viability. [e] Equilibrium dialysis between buffer and rat brain homogenate. [f] GreenScreen HC assay, see reference 51.

To evaluate receptor occupancy in rat CNS from an oral dose, **25** was advanced to an *ex vivo* autoradiography experiment. Male Sprague-Dawley rats were dosed orally with vehicle alone (10% DMA, 10% Solutol HS15, 80% (10% aqueous (2-hydroxypropyl)-*β*-cyclodextrin)) or **25** (1, 3 or 10 mg/kg, po) and sacrificed 1 h post-dose. Sections of the hippocampal CA3 region were prepared and incubated with [^{3}H]-M-MPEP,[34] with levels of bound radioactivity in the sections determined using a beta imager. Receptor occupancy was determined from mean

specific binding with the vehicle treated control taken as 100%. As depicted in Figure 2, **25** demonstrated excellent, dose-dependent, occupancy of $mGlu_5$ receptors from an oral dose, with an estimated ED_{50} of 0.3 mg/kg. By comparison mavoglurant returned an ED_{50} of approximately 3.6 mg/kg po in a comparable study.

Figure 2. [^{3}H]-M-MPEP *ex vivo* autoradiography in rat hippocampal CA3 region 1 hour following oral administration of **25**.[a]

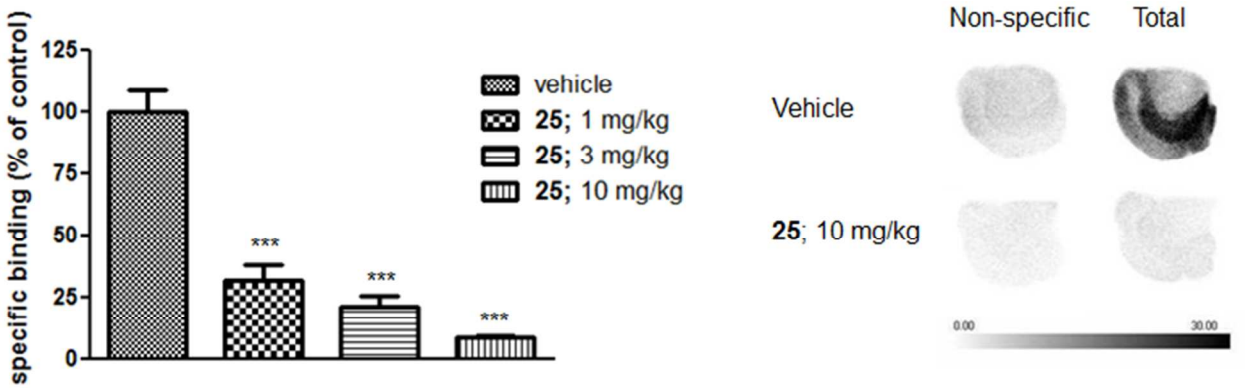

[a] Results are expressed as mean specific binding as a percentage of control taken as 100% (n=5). For statistical analyses data were square root transformed and analysed by one-way analysis of variance followed by Williams' test to compare **25** to vehicle. ***p<0.001. The images are autoradiograms of coronal half-brain sections in rat hippocampal CA3 sections and are representative samples of the 10 mg/kg treatment group.

The encouraging overall profile and high receptor occupancy of **25** prompted us to take the compound forward into a preliminary assessment of rat repeat dose toxicology. Material for the study was synthesized using the route depicted in Scheme 2 with Negishi coupling replacing Stille coupling as the final step, negating the use of stoichiometric tin in the synthesis, and the batch used was confirmed to have acceptable levels of Pd (< 0.5 mg/kg) by inductively coupled plasma-mass spectrometry (ICP-MS) analysis. A non-GLP 7-day repeat dose toxicity study in Sprague-Dawley rats was performed, administering **25** by once daily oral gavage at levels of 3,

10 and 30 mg/kg/day. **25** was well tolerated, no target organ effects were observed, no clinical observations or differences in body weight, food consumption, haematology, coagulation, clinical chemistry, urinalysis, organ weights, gross pathology or histopathological findings that were considered to be related to treatment with test compound were observed.

As an initial *in vivo* evaluation of **25** we undertook a murine study in a marble burying paradigm, a model which has been used to probe the anti-anxiolytic effect of $mGlu_5$ NAMs.[55,56] In brief, 24 marbles were evenly spaced across the surface of sawdust bedding, and male CD-1 mice treated orally with vehicle (10% Solutol HS15, 90% (10% aqueous (2-hydroxypropyl)-β-cyclodextrin)) or **25** (1, 3, 10 or 30 mg/kg) thirty minutes before the start of the test. After pre-treatment, mice were placed individually in a cage containing the marbles, and after thirty minutes mice were removed and the number of marbles buried by at least two thirds into the sawdust were counted. Compound **25** was able to strongly attenuate marble burying behavior in a dose dependent manner, with an estimated ED_{50} of approximately 8 mg/kg, comparable to that of mavoglurant **1** in our hands in the same model.

In conclusion, stabilization of the $mGlu_5$ receptor enabled a fragment screen, leading to the identification of pyrimidine hit **5** which was then optimized using a SBDD approach to a highly potent series of negative allosteric modulators. During the course of the project, multiple crystal structures of $mGlu_5$ NAMs were generated, including those of **14** and **25**. As well as their utility in the lead optimization process these structures also help to explain several of the inherent challenges in drug discovery in this area, and pave the way for future SBDD campaigns in the mGlu field. Compound **25**, hereafter known as HTL14242, is a high affinity modulator of $mGlu_5$

with excellent *in vitro* characteristics including high selectivity within the metabotropic family of GPCRs. HTL14242 has good PK characteristics in rat and dog, high receptor occupancy as elucidated through *ex vivo* autoradiography studies, demonstrates activity *in vivo* in a relevant model, and has a clean profile in a repeat dose rat toxicology study. Based on the studies described in this manuscript, HTL14242 has been selected as an advanced lead compound for further development.

EXPERIMENTAL SECTION

Chemistry

Active compounds have been examined for known classes of assay interference compounds and do not fall into this category.[57] ^{19}F NMR data for **25**, HTL14242 is referenced to $C_6H_5CF_3$ at -63.72 ppm. ^{1}H NMR and LCMS QC data for all compounds, and experimental procedures for synthesized compounds in Tables 1 and 2 are described in the Supporting Information. Synthesis of **25**, HTL14242 is described below.

3-(5-Amino-2-chloropyridin-4-yl)-5-chlorobenzonitrile. A mixture of 4,6-dichloropyrimidine (9.0 g, 60.4 mmol), 3-chloro-5-(4,4,5,5-tetramethyl-1,3,2-dioxaborolan-2-yl)benzonitrile (17.6 g, 66.8 mmol) and cesium carbonate (35.0 g, 107.4 mmol) were dissolved in 1,4-dioxane / water (9:1, 50 mL). After degassing with N_2, Pd(dppf)Cl_2 (2.20 g, 3.0 mmol) was added and the reaction mixture was stirred at 90°C for 2 h. After cooling to rt the reaction mixture was partitioned between H_2O (250 mL) and EtOAc (150 mL), the phases were separated and the aqueous layer extracted with EtOAc (2 x 150 mL). The combined organic layers were dried (Na_2SO_4), concentrated *in vacuo* and purification by column chromatography (SiO_2, 0 to 10% ethyl acetate in hexane) yielded the title compound (4.0 g, 16.0 mmol) as off-white solid. m/z 250.1 $(M+H)^+$; δ_H (400 MHz; d_6-DMSO) 8.27 (s, 1H), 8.53 (s, 1H), 8.59 (s, 1H), 8.66 (s, 1H), 9.16 (s, 1H).

3-Chloro-5-[6-(5-fluoropyridin-2-yl)pyrimidin-4-yl]benzonitrile (**25**, HTL14242).

A mixture of 2-bromo-5-fluoropyridine (500 mg, 2.89 mmol) and hexamethylditin (946 mg, 2.89 mmol) in DME (10 mL) was degassed by purging with N_2 for 5 min before the addition of

tetrakis(triphenylphosphine)palladium(0) (166 mg, 0.14 mmol). The reaction mixture was stirred at 110 °C for 16 h before cooling to rt and partitioning between H_2O (50 mL) and EtOAc (25 mL). The phases were separated and the aqueous phase was extracted with EtOAc (2 x 25 mL). The combined organic phases were dried (Na_2SO_4) and concentrated *in vacuo* to yield crude 5-fluoro-2-(trimethylstannyl)pyridine (700 mg) which was used in the subsequent step without characterization or further purification. 3-Chloro-5-(6-chloropyrimidin-4-yl)benzonitrile (100 mg, 0.39 mmol) and crude 5-fluoro-2-(trimethylstannyl)pyridine (114 mg) were dissolved in toluene (15 mL) and the reaction mixture was degassed by purging with N_2 for 5 min before the addition of tetrakis(triphenylphosphine)palladium(0) (46.2 mg, 0.04 mmol) and copper(I) iodide (7.6 mg, 0.03 mmol). The reaction mixture was stirred at 110 °C for 16 h before cooling to rt and partitioning between H_2O (50 mL) and EtOAc (25 mL). The phases were separated and the aqueous phase was extracted with EtOAc (2 x 25 mL). The combined organic phases were dried (Na_2SO_4) and concentrated *in vacuo*. Purification by gradient flash chromatography, eluting with 0-10% EtOAc in hexane yielded the title compound (37 mg, 0.12 mmol) as a pale yellow solid. *m/z* 311.0, 313.0 $(M+H)^+$; ^{1}H NMR (400 MHz, DMSO) δ: 8.02 (td, *J* = 8.7, 2.7 Hz, 1H), 8.29 (dd, *J* = 2.0, 1.4 Hz, 1H), 8.57-8.67 (m, 2H), 8.76 (t, *J* = 1.5 Hz, 1H), 8.84 (d, *J* = 2.7 Hz, 1H), 8.95 (d, *J* = 1.5 Hz, 1H), 9.44 (d, *J* = 1.2 Hz, 1H); ^{19}F NMR (376 MHz, DMSO) δ: -125.85 (dd, *J* = 8.6, 4.6 Hz, 1F); ^{13}C NMR (101 MHz,) δ: 113.1, 114.1, 117.1, 123.6 (d, $^3J_{CF}$ = 5.4 Hz, 1C), 124.6 (d, $^2J_{CF}$ = 19.2 Hz, 1C), 129.7, 131.5, 134.0, 134.9, 138.2 (d, $^2J_{CF}$ = 24.5 Hz, 1C), 139.0, 149.4 (d, $^4J_{CF}$ = 3.8 Hz, 1C), 158.9, 160.5 (d, $^1J_{CF}$ = 258.4 Hz, 1C), 160.8, 162.5.

Expression of $mGlu_5$ and Membrane Preparation

cDNA encoding the human $mGlu_5$ receptor was transfected into HEK293 cells using the transfection reagent Genejuice (Novagen). Forty-eight hours after transfection, cells were harvested and washed twice with ice cold phosphate-buffered saline. Membranes were prepared and stored as previously described.[58]

[^{3}H]-M-MPEP binding assay

Membranes (2.5 μg) prepared from HEK293 cells stably expressing the $mGlu_5$ receptor were incubated with a K_D concentration (~0.75 nM) of [^{3}H]-M-MPEP[34] in binding buffer (50 mM HEPES; 150 mM NaCl; pH 7.4). Nonspecific binding was determined by inclusion of 0.1 mM of MPEP. After 90 min incubation at room temperature (25 °C) assays were terminated by rapid filtration through 96-well GF/B filter plates pre-soaked with 0.1% polyethyleneimine (PEI) using a 96-well head harvester (Tomtec, USA) and plates washed 5 × 0.5 mL with H_2O. Scintillant (50 μL Ultima Gold F; PerkinElmer, UK) was added and bound radioactivity was determined using scintillation spectroscopy on a Microbeta counter (PerkinElmer, UK). Inhibition binding curves were fitted to a four-parameter logistic equation to determine IC_{50} values. IC_{50} values were converted to K_i values with the Cheng-Prusoff equation[59] using a K_D value (0.75 nM) derived from saturation binding studies.

Functional assay

To measure receptor activation the IPone assay kit from Cisbio (France) was used. The assay was optimised to measure the ability (potency; pIC_{50}) of antagonists / negative allosteric

modulators to reduce agonist (L-quisqualic acid) induced inositol phosphate turnover. Briefly, 16 h prior to the assay HEK293 cells stably expressing $mGlu_5$ were plated at a density of 35,000 cells/well in half-area 96-well plates. On the day of the assay media was removed and replaced with IPone assay buffer (supplied in the assay kit) supplemented with 5 mM sodium pyruvate and 2 μL/mL glutamate pyruvate transaminase (to breakdown endogenous glutamate) and plates were incubated at 37°C for 45 min prior to the addition of test compound. 15 min after addition of test compound an EC_{80} concentration of L-quisqualic acid (~ 0.32 μM) was added. The assay was incubated for 30 min at 37 °C before termination and reading as per manufacturer's instructions.

Expression, Membrane Preparation, Protein Purification and Crystallization of Thermostabilized $mGlu_5$.

The $mGlu_5$-StaR (as detailed in reference 11 with an additional four amino acid truncation at the C-terminus) carrying an N-terminal GP64 signal sequence and a C-terminal deca histidine-tag was expressed in *Sf21* cells grown in ESF921 medium supplemented with 10% (v/v) FBS and 1% (v/v) penicillin/streptomycin using the FastBac expression system (Invitrogen). Cells were infected at a density of 2 x 10^6 cells/mL with baculovirus at an approximate multiplicity of infection of 1. Cultures were grown at 27 ˚C and harvested 48 h post infection.

All subsequent purification steps were carried out at 4 °C. To prepare membranes, two litres of cells were re-suspended in PBS buffer supplemented with protease inhibitor tablets and 5 mM EDTA. Cells were disrupted by micro-fluidizer at 60 PSI and membranes collected by ultracentrifugation at 204.7k x *g* for 1 h. Membranes were washed with PBS buffer

supplemented with protease inhibitor tablets and 500 mM NaCl, collected by ultracentrifugation and re-suspended in 40 mM HEPES pH 7.5, 250 mM NaCl and stored at -80 °C. Just prior to solubilization membranes were thawed, homogenized, supplemented with 40 μM **14** or 25 μM **25** and 8 mM iodoacetamide, and incubated on a roller mixer for 40 minutes. Membranes were solubilized with 1.5% (w/v) DDM for 1 h, insoluble material was removed by ultra-centrifugation and the solubilized lysate batch bound to 10 mL of Ni-NTA Superflow resin (Qiagen) for 2.5 h in the presence of 10 mM imidazole. Resin was washed with a gradient of 10 to 50 mM imidazole in 40 mM HEPES pH 7.5, 250 mM NaCl, 0.05% (w/v) DDM, and 20 μM **14** or 12.5 μM **25** over 35 column volumes before bound material was eluted in a step with 245 mM imidazole. Receptor was further purified by gel filtration (SEC) in 40 mM HEPES pH 7.5, 150 mM NaCl, 0.03% (w/v) DDM, and 10 μM **14** or 12.5 μM **25**. Receptor purity was analyzed using SDS-PAGE and LC-MS, and receptor monodispersity was assayed by analytical SEC. Protein concentration was determined using the receptor's calculated extinction coefficient at 280 nm ($\varepsilon_{280,\,calc}$ = 61770 (mg/mL x cm)$^{-1}$) and confirmed by quantitative amino acid analysis.

$mGlu_5$-StaR was crystallized in LCP at 20 °C. The protein was concentrated to ~40 mg/mL **14** and ~50 mg/mL **25** and mixed with monoolein (Nu-Check) supplemented with 10% (w/w) cholesterol (Sigma Aldrich) and 100 μM **14** or **25** using the twin-syringe method.[60] The final protein:lipid ratio was 40:60 (w/w). 40 nL boli were dispensed on 96-well glass bases and overlaid with 750 nL precipitant solution using a Mosquito LCP from TTPLabtech. 40 μm plate shaped crystals of $mGlu_5$-StaR in complex with **14** or **25** were grown in 100 mM 2-ethanesulphonic acid (MES) across a pH range of 5.5-6.8, 100-250 mM $(NH_4)_2HPO_4$, 24-34% (v/v) polyethylene glycol 400, and supplemented with either 100 μM **14** or **25**. A complete dataset to 2.60 Å for $mGlu_5$-StaR-**25** was obtained by merging diffraction data from 9 crystals

belonging to the monoclinic spacegroup C121. A complete dataset to 3.10 Å for $mGlu_5$-StaR-**14** was also obtained by merging diffraction data from 9 crystals belonging to the monoclinic spacegroup C121. It was possible to mount single crystals for data collection, which were flash-cooled and stored in liquid nitrogen.

Diffraction Data Collection, Processing, Structure Solution, Refinement and Analysis

X-ray diffraction data were measured on a Pilatus 6M hybrid-pixel detector at Diamond Light Source beamline I24 using a 10 μm diameter beam. Data from individual crystals was integrated using XDS.[61] Data merging and scaling was carried out using the program AIMLESS.[62] Data collection statistics are reported in Supporting Information Table 3.

The structure was solved by molecular replacement using the program *Phaser*[38] searching for one copy of the $mGlu_5$ mavoglurant co-structure (PDB ID: 4OO9). Manual model building was performed in *COOT*[63] using sigma-A weighted $2m|F_o|-|DF_c|$, $m|F_o|-D|F_c|$ maps calculated in Phenix.[37] Refinement of both structures was performed using *Phenix.refine*[64] implementing a combination of positional and individual isotropic b-factor refinement. Structure quality was assessed with MolProbity.[65] Refinement statistics are presented in Supporting Information Table 3.

Structures were superposed and aligned for comparison purposes using *COOT* [63] to generate global structural superpositions**.** Local R.M.S.D. analysis between the different $mGlu_5$-StaR structures was calculated using Superpose from the CCP4 suite of programs.[39] Figures were prepared using *PyMOL* (Schrödinger).[66]

Co-ordinates and structure factors have been deposited in the Protein Data Bank under the accession codes 5CGC (Compound **14**) and 5CGD (Compound **25**).

ASSOCIATED CONTENT

Supporting Information. Supplier information or synthetic details for preparation of intermediates and final compounds, LCMS QC data for all compounds, NMR data for synthesized compounds, crystallographic information table, selectivity data for **25**, HTL14242, *ex vivo* autoradiography and *in vivo* mouse marble burying experimental details. This material is available free of charge via the Internet at http://pubs.acs.org.

AUTHOR INFORMATION

Author Contributions

The manuscript was written through contributions of all authors. All authors have given approval to the final version of the manuscript.

Notes

The authors declare no competing financial interests.

ACKNOWLEDGMENTS

The authors express their gratitude to Giles A. Brown for assistance with radioligand and literature compound synthesis. James Dolan and Nathan Bartlett at Key Organics Ltd are acknowledged for the tin free synthesis of **25**. Liz Jagger and colleagues at RenaSci Ltd, and Vivian Costantini and colleagues at Aptuit (Verona) Srl., are acknowledged for generation of *ex vivo* autoradiography data and mouse marble burying data respectively, Katarzyna Dymarkowska and colleagues at Charles River Laboratories are acknowledged for generation of rat repeat dose toxicology data, as is Mark Maginn for overseeing the study on behalf of Heptares.

ABBREVIATIONS

VE-TPGS, D-α-tocopheryl polyethylene glycol 1000 succinate; TMD, Transmembrane Domain

REFERENCES

1. Nakanishi, S. Molecular diversity of glutamate receptors and implications for brain function. *Science* **1992**, *258*, 597-603.

2. Conn, P. J.; Pin, J. P. Pharmacology and functions of metabotropic glutamate receptors. *Annu. Rev. Pharmacol. Toxicol*. **1997**, *37*, 205-237.

3. Shigemoto, R.; Mizuno, N. Metabotropic glutamate receptors – imunocytochemical and in situ hybridization analyses. In *Handbook of Chemical Neuroanatomy*; Ottersen, O. P., Storm-Mathisen, J., Eds.; Elsevier: Amsterdam, 2000; Vol. 18, pp 63-98.

4. Bennett, K. A.; Doré, A. S.; Christopher, J. A.; Weiss, D. R.; Marshall, F. H. Structures of mGluRs shed light on the challenges of drug development of allosteric modulators. *Curr. Opin. Pharmacol*. **2015**, *20*, 1-7.

5. Celanire, S.; Sebhat, I.; Wichmann, J.; Mayer, S.; Schann, S.; Gatti, S. Novel metabotropic glutamate receptor 2/3 antagonists and their therapeutic applications: a patent review (2005 - present). *Expert Opin. Ther. Patents* **2015**, *25*, 69-90.

6. Emmitte, K. A. Recent Advances in the Design and Development of Novel Negative Allosteric Modulators of $mGlu_5$. *ACS Chem. Neurosci*. **2011**, *2*, 411–432.

7. Emmitte, K. A. $mGlu_5$ negative allosteric modulators: a patent review (2010 - 2012). *Expert Opin. Ther. Patents* **2013**, *23*, 393-408.

8. Hao, J.; Xiong, H. SAR Studies on $mGlu_5$ Receptor Positive Allosteric Modulators (2003- 2013). *Curr. Top. Med. Chem*. **2014**, *14*, 1789-1841.

9. Probe Reports from the NIH Molecular Libraries Program, Pure Positive Allosteric Modulators (PAMs) of mGlu5 with Competitive MPEP-Site Interaction. http://www.ncbi.nlm.nih.gov/books/NBK143535 (accessed May 28, 2015).

10. Noetzel, M. J.; Gregory, K. J.; Vinson, P. N.; Manka, J. T.; Stauffer, S. R.; Lindsley, C. W.; Niswender, C. M.; Xiang, Z.; Conn, P. J. A Novel Metabotropic Glutamate Receptor 5 Positive Allosteric Modulator Acts at a Unique Site and Confers Stimulus Bias to mGlu5 Signalings. *Mol. Pharmacol*. **2013**, *83*, 835–847.

11. Doré, A. S.; Okrasa, K.; Patel, J. C.; Serrano-Vega, M.; Bennett, K.; Cooke, R. M.; Errey, J. C.; Jazayeri, A.; Khan, S.; Tehan, B.; Weir, M.; Wiggin, G. R.; Marshall, F. H. Structure of class C GPCR metabotropic glutamate receptor 5 transmembrane domain. *Nature* **2014**, *511*, 557-562.

12. Jacquemont, S.; Curie, A.; des Portes, V.; Torrioli, M. G.; Berry-Kravis, E.; Hagerman, R. J.; Ramos, F. J.; Cornish, K.; He, Y.; Paulding, C.; Neri, G.; Chen, F.; Hadjikhani, N.; Martinet, D.; Meyer, J.; Beckmann, J. S.; Delange, K.; Brun, A; Bussy, G.; Gasparini, F.; Hilse, T.; Floesser, A.; Branson, J.; Bilbe, G.; Johns, D.; Gomez-Mancilla, B. Epigenetic modification of the FMR1 Gene in Fragile X syndrome is associated with differential response to the mGluR5 antagonist AFQ056. *Sci. Transl. Med.* **2011**, *3*, 64ra1.

13. Berg, D.; Godau, J.; Trenkwalder, C.; Eggert, K.; Csoti, I.; Storch, A.; Huber, H.; Morelli-Canelo, M.; Stamelou, M.; Ries, V.; Wolz, M.; Schneider, C.; Di Paolo, T.; Gasparini, F.; Hariry, S.; Vandemeulebroecke, M.; Abi-Saab, W.; Cooke, K.; Johns, D.; Gomez-Mancilla, B. AFQ056 treatment of levodopa-induced dyskinesias: results of 2 randomized controlled trials. *Mov. Disord.* **2011**, *26*, 1243-1250.

14. Penknold, J. C.; McClure, D. J.; Appeltauer, L; Wrzesinski, L.; Allan, T. Treatment of Anxiety Using Fenobam (a Nonbenzodiazepine) in a Double-blind Standard (Diazepam) Placebo-controlled Study. *J. Clin. Psychopharmacol*. **1982**, *2*, 129-133.

15. Zerbib, F.; Bruley des Varannes, S.; Roman, S.; Tutuian, R.; Galmiche, J. P.; Mion, F.; Tack, J.; Malfertheiner, P.; Keywood, C. Randomised clinical trial: effects of monotherapy with ADX10059, a mGluR5 inhibitor, on symptoms and reflux events in patients with gastro-oesophageal reflux disease. *Aliment. Pharmcol. Ther.* **2011**, *33*, 911-921.

16. Kalliomäki, J.; Huizar, K.; Kågedal. M.; Hägglöf, B.; Schmelz, M. Evaluation of the effects of the metabotropic glutamate receptor 5-antagonist on the electrically induced pain and central sensitization in healthy human volunteers. *Eur. J. Pain* **2013**, *17*, 1465-1471.

17. Study to Evaluate the Effect of AFQ056 in Obsessive Compulsive Disorder (OCD) Patients Resistant to Selective Serotonin Reuptake Inhibitor (SSRI) Therapy (NCT01813019). https://clinicaltrials.gov/ct2/show/NCT01813019 (Accessed May 28, 2015).

18. Marin, J. C.; Goadsby, P. J. Glutamatergic fine tuning with ADX-10059: a novel therapeutic approach for migrane? *Expert Opin. Investig. Drugs* **2010**, *19*, 555-561.

19. Reilman, R.; Rouzade-Dominquez, M-L.; Saft, C.; Süssmuth, S. D.; Priller, J.; Rosser, A.; Rickards, H.; Schöls, L.; Pezous, N.; Gasparini, F.; Johns, D.; Landwehrmeyer, G. B.; Gomez-Mancilla, B. A randomized, placebo-controlled trial of AFQ056 for the treatment of chorea in Huntington's disease. *Mov. Disord.* **2015**, *30*, 427-431.

20. Quiroz, J. A.; Tamburri, P.; Deptula, D.; Banken, L.; Beyer, U.; Fontoura, P; Santarelli, L. The efficacy and safety of basimglurant as adjunctive therapy in major depression; a randomised, double-blind, placebo-controlled study. *Eur. Neuropsychopharmacol.* **2014**, *24* (Suppl. 2), S468.

21. Lindemann, L.; Porter, R. H.; Scharf, S. H.; Kuennecke, B.; Bruns, A.; von Kienlin, M.; Harrison, A. C.; Paehler, A.; Funk, C.; Gloge, A.; Schneider, M.; Parrott, N. J.; Polonchuk, L.; Niederhauser, U.; Morairty, S. R.; Kilduff, T. S.; Vieira, E.; Kolczewski, S.; Wichmann, J.; Hartung, T.; Honer, M.; Borroni, E.; Moreau, J.-L.; Prinssen, E.; Spooren, W.; Wettstein, J. G.; Jaeschke, G. Pharmacology of Basimglurant (RO4917523, RG7090), a Unique Metabotropic

Glutamate Receptor 5 Negative Allosteric Modulator in Clinical Development for Depression. *J. Pharmacol. Exp. Ther*. **2015**, *353*, 213-233.

22. Scharf, S. H.; Jaeschke, G.; Wettstein, J. G.; Lindemann, L. Metabotropic glutamate receptor 5 as drug target for Fragile X syndrome. *Curr. Opin. Pharmacol.* **2015**, *20*, 124-134.

23. Kalgutkar, A. S.; Gardner, I.; Obach, R. S.; Shaffer, C. L.; Callegari, E.; Henne, K. R.; Mutlib, A. E.; Dalvie, D. K.; Lee, J. S.; Nakai, Y.; O'Donnell, J. P.; Boer, J.; Harriman, S. P. A Comprehensive Listing of Bioactivation Pathways of Organic Functional Groups. *Curr. Drug. Metab*. **2005**, *6*, 161-225.

24. Hughes, Z. A.; Neal, S. J.; Smith, D. L.; Rizzo, S. J.; Pulicicchio, C. M.; Lotarski, S.; Lu, S.; Dwyer, J. M.; Brennan, J.; Olsen, M.; Bender, C. N.; Kouranova, E.; Andree, T. H.; Harrison, J. E.; Whiteside, G. T.; Springer, D.; O'Neil, S. V.; Leonard, S.; Schechter, L. E.; Dunlop, J.; Rosenzweig-Lipson, S.; Ring, R. H. Negative allosteric modulation of metabotropic glutamate receptor 5 results in broad spectrum activity relevant to treatment resistant depression. *Neuropharmacology* **2013**, *66*, 202-214.

25. Sperry, J. B.; Farr, R. M.; Levent, M.; Ghosh, M.; Hoagland, S. M.; Varsolona, R. J.; Sutherland, K. A robust process for an mGluR5 negative allosteric modulator: difluoromethylation and Sonogashira coupling on large scale. *Org. Process Res. Dev*. **2012**, *16*, 1854-1860.

26. Zhang, L.; Balan, G.; Barreiro, G.; Boscoe, B. P.; Chenard, L. K.; Cianfrogna, J.; Claffey, M. M.; Chen, L.; Coffman, K. J.; Drozda, S. E.; Dunetz, J. R.; Fonseca, K. R.; Galatsis, P.; Grimwood, S.; Lazzaro, J. T.; Mancuso, J. Y.; Miller, E. L.; Reese, M. R.; Rogers, B. N.; Sakurada, I.; Skaddan, M.; Smith, D. L.; Stepan, A. F.; Trapa, P.; Tuttle, J. B.; Verhoest, P. R.;

Walker, D. P.; Wright, A. S.; Zaleska, M. M.; Zasadny, K.; Shaffer, C. L. The discovery and preclinical characterization of 1-methyl-3-(4-methylpyridin-3-yl)-6-(pyridin-2-ylmethoxy)-1*H*-pyrazolo[3,4-*b*]pyrazine (PF470), a highly potent, selective and efficacious metabotropic glutamate receptor 5 (mGluR5) negative allosteric modulator. *J. Med. Chem.* **2014**, *57*, 861-877.

27. Zhuo, X.; Huang, X. S.; Degnan, A. P.; Snyder, L. B.; Yang, F.; Huang, H.; Shu, Y.-Z.; Johnson, B. M. Identification of Glutathione Conjugates of Acetylene-Containing Positive Allosteric Modulators of Metabotropic Glutamate Receptor Subtype 5. *Drug Metab. Dispos*. **2015**, *43*, 578-589.

28. Addex Therapeutics Press Release: Development of ADX10059 Ended for Long-term Use. http://www.addextherapeutics.com/investors/press-releases/news-details/?tx_ttnews%5Btt_news%5D%20%20=%2088&cHash=d075a6fa63acce925582f8f481fb8dc3 (accessed May 28, 2015).

29. Andrews, S. P.; Brown, G. A.; Christopher, J. A. Structure-Based and Fragment-Based GPCR Drug Discovery. *ChemMedChem* **2014**, *9*, 256-275.

30. Jhoti, H.; Williams, G.; Rees, D. C.; Murray, C. W. The 'rule of three' for fragment-based drug discovery: where are we now? *Nat. Rev. Drug Discovery* **2013**, *12*, 644−645.

31. Joseph-McCarthy, D.; Campbell, A. J.; Kern, G.; Moustakas, D. Fragment-Based Lead Discovery and Design. *J. Chem. Inf. Model*. **2014**, *54*, 693-704.

32. Ferenczy, G. G.; Keserű, G. M. How Are Fragments Optimized? A Retrospective Analysis of 145 Fragment Optimizations. *J. Med. Chem.* **2013**, *56*, 2478-2486.

33. Christopher, J. A.; Brown, J.; Doré, A. S.; Errey, J. C.; Koglin, M.; Marshall, F. H.; Myszka, D. G.; Rich, R. L.; Tate, C. G.; Tehan, B.; Warne, T.; Congreve, M. Biophysical Fragment Screening of the β_1-Adrenergic Receptor: Identification of High Affinity Arylpiperazine Leads Using Structure-Based Drug Design. *J. Med. Chem.* **2013**, *56*, 3446-3455.

34. Gasparini, F.; Andres, H.; Flora, P. J.; Heinrich, M.; Inderbitzin, M.; Lingenhöhl, K.; Müller, H.; Munk, V. C.; Omilusik, K.; Stierlin, C.; Stoehr, N.; Vranesic, I.; Kuhn, R. [^{3}H]-M-MPEP, a Potent, Subtype-Selective Radioligand for the Metabotropic Glutamate Receptor Subtype 5. *Bioorg. Med. Chem. Lett*. **2002**, *12*, 407-409.

35. Ligand efficiency LE = −RT(ln K_i)/N, where N is the number of heavy atoms. Hopkins, A. L.; Groom, C. R.; Alex, A. Ligand efficiency: a useful metric for lead selection. *Drug Discovery Today* **2004**, *9*, 430−443.

36. Christopher, J. A.; Congreve, M. S.; Aves, S. J.; Tehan, B. G. 4-(3-Cyanophenyl)-6-pyridinylpyrimidine $mGlu_5$ modulators. PCT Patent Appl. WO2015/008073 A1, Jan 22 2015.

37. Adams, P. D.; Afonine, P. V.; Bunkóczi, G.; Chen, V. B.; Davis, I. W.; Echols, N.; Headd, J. J.; Hung, L.-W.; Kapral, G. J.; Grosse-Kunstleve, R. W.; McCoy, A. J.; Moriarty, N. W.; Oeffner, R.; Read, R. J.; Richardson, D. C.; Richardson, J. S.; Terwilliger, T. C.; Zwart, P. H. PHENIX: a comprehensive Python-based system for macromolecular structure solution. *Acta Crystallogr*. **2010**, *D66*, 213-221.

38. McCoy, A. J.; Grosse-Kunstleve, R. W.; Adams, P. D.; Winn, M. D.; Storoni, L. C.; Read, R. J. Phaser crystallographic software. *J. Appl. Cryst*. **2007**, *40*, 658-674.

39. Collaborative Computational Project, Number 4. The CCP4 Suite: Programs for Protein Crystallography. *Acta Crystallogr.* **1994**, *D50*, 760-763.

40. Ballesteros, J. A.; Weinstein, H. Integrated methods for the construction of three-dimensional models and computational probing of structure−function relations in G protein-coupled receptors. *Methods Neurosci*. **1995**, *25*, 366−428.

41. Anighoro, A.; Graziani, D.; Bettinelli, I.; Cilia, A.; De Toma, C.; Longhi, M.; Mangiarotti, F.; Menegon, S.; Pirona, L.; Poggesi, E.; Riva, C.; Rastelli, G. Insights into the interaction of negative allosteric modulators with the metabotropic glutamate receptor 5: Discovery and computational modeling of a new series of ligands with nanomolar affinity. *Bioorg. Med. Chem.* **2015**, *23*, 3040-3058.

42. Wood, M. R.; Hopkins, C. R.; Brogan, J. T.; Conn, P. J.; Lindsley, C. W. "Molecular Switches" on mGluR Allosteric Ligands That Modulate Modes of Pharmacology. *Biochemistry* **2011**, *50*, 2403–2410.

43. Sams, A. G.; Mikkelsen, G. K.; Brodbeck, R. M.; Pu, X.; Ritzén, A. Efficacy switching SAR of mGluR5 allosteric modulators: Highly potent positive and negative modulators from one chemotype. *Bioorg. Med. Chem. Lett*. **2011**, *21*, 3407–3410.

44. Vanejevs, M.; Jatzke, C.; Renner, S.; Müller, S.; Hechenberger, M.; Bauer, T.; Klochkova, A.; Pyatkin, I.; Kazyulkin, D.; Aksenova, E.; Shulepin, S.; Timonina, O.; Haasis, A.; Gutcaits, A.; Parsons, C. G.; Kauss, V.; Weil, T. Positive and Negative Modulation of Group I Metabotropic Glutamate Receptors. *J. Med. Chem*. **2008**, *51*, 634–647.

45. O'Brien, J. A.; Lemaire, W.; Chen, T.-B.; Chang, R. S. L.; Jacobson, M. A.; Ha, S. N.; Lindsley, C. W.; Schaffhauser, H. J.; Sur, C.; Pettibone, D. J.; Conn, P. J.; Williams, D. L., Jr. A family of highly selective allosteric modulators of the metabotropic glutamate receptor subtype 5. *Mol. Pharmacol*. **2003**, *64*, 731-740.

46. Engers, D. W.; Rodriguez, A. L.; Williams, R.; Hammond, A. S.; Venable, D.; Oluwatola, O.; Sulikowski, G. A.; Conn, P. J.; Lindsley, C. W. Synthesis, SAR and unanticipated pharmacological profiles of analogues of the mGluR5 ago-potentiator ADX-47273. *ChemMedChem* **2009**, *4*, 505-511.

47. Lamb, J. P.; Engers, D. W.; Niswender, C. M.; Rodriguez, A. L.; Venable, D. F.; Conn, P. J.; Lindsley, C. W. Discovery of molecular switches within the ADX-47273 mGlu5 PAM scaffold that modulate modes of pharmacology to afford potent mGlu5 NAMs, PAMs and partial antagonists. *Bioorg. Med. Chem. Lett.* **2011**, *21*, 2711-2714.

48. Rankovic, Z. CNS Drug Design: Balancing Physicochemical Properties for Optimal Brain Exposure. *J. Med. Chem*. **2015**, *56*, 2584–2608.

49. Rat iv/po PK data for dipraglurant were generated by Heptares using 1 mg/kg iv and 2 mg/kg po doses in 10% DMA + 10% Solutol HS15 + 80% Saline.

50. Vranesic, I.; Ofner, S.; Flor, P. J.; Bilbe, G.; Bouhelal, R.; Enz, A.; Desrayaud, S.; McAllister, K.; Kuhn, R.; Gasparini, F. AFQ056/mavoglurant, a novel clinically effective mGluR5 antagonist: Identification, SAR and pharmacological characterization. *Bioorg. Med. Chem.* **2014**, *22*, 5790-5803.

51. Walmsley, R. M.; Tate, M. The GADD45a-GFP GreenScreen HC Assay. *Methods Mol. Biol*. **2012**, *817*, 231-250.

52. Raboisson, P.; Breitholtz-Emanuelsson, A.; Dahllöf, H.; Edwards, L.; Heaton, W. L.; Isaac, M.; Jarvie, K.; Kers, A.; Minidis, A. B. E.; Nordmark, A.; Sheehan, S. M.; Slassi, A.; Ström, P.; Terelius, Y.; Wensbo, D.; Wilson, J. M.; Xin, T.; McLeod, D. A. Discovery and characterization of AZD9272 and AZD6538—Two novel mGluR5 negative allosteric modulators selected for clinical development. *Bioorg. Med. Chem. Lett*. **2012**, *22*, 6974-6979.

53. Mueller, R.; Dawson, E. S.; Meiler, J.; Rodriguez, A. L.; Chauder, B. A.; Bates, B. S.; Felts, A. S.; Lamb, J. P.; Menon, U. N.; Jadhav, S. B.; Kane, A. S.; Jones, C. K.; Gregory, K. J.; Niswender, C. M.; Conn, P. J.; Olsen, C. M.; Winder, D. G.; Emmitte, K. A.; Lindsley, C. W. Discovery of 2-(2-Benzoxazoyl amino)-4-Aryl-5-Cyanopyrimidine as Negative Allosteric Modulators (NAMs) of Metabotropic Glutamate Receptor 5 ($mGlu_5$): From an Artificial Neural Network Virtual Screen to an In Vivo Tool Compound. *ChemMedChem* **2012**, *7*, 406-414.

54. Felts, A. S.; Rodriguez, A. L.; Morrison, R. D.; Venable, D. F.; Manka, J. T.; Bates, B. S.; Blobaum, A. L.; Byers, F. W.; Daniels, J. S.; Niswender, C. M.; Jones, C. K.; Conn, P. J.; Lindsley, C. W.; Emmitte, K. A. *Bioorg. Med. Chem. Lett*. **2013**, *23*, 5779-5785.

55. Spooren, W. P.; Vassout, A.; Neijt, H. C.; Kuhn, R.; Gasparini, F.; Roux, S.; Porsolt, R. D.; Gentsch, C. Anxiolytic-Like Effects of the Prototypical Metabotropic Glutamate Receptor 5 Antagonist 2-Methyl-6-(phenylethynyl)pyridine in Rodents. *J. Pharmacol. Exp. Ther.* **2000**, *295*, 1267-1275.

56. Zhou, H.; Topiol, S. W.; Grenon, M.; Jimenez, H. N.; Uberti, M. A.; Smith, D. G.; Brodbeck, R. M.; Chandrasena, G.; Pedersen, H.; Madsen, J. C.; Doller, D.; Li, G. Discovery and structure–activity relationship of 1,3-cyclohexyl amide derivatives as novel mGluR5 negative allosteric modulators. *Bioorg. Med. Chem. Lett.* **2013**, *23*, 1398-1406.

57. Baell, J. B.; Holloway, G. A. *J. Med. Chem*. **2010**, *53*, 2719-2740.

58. Robertson, N.; Jazayeri, A.; Errey, J.; Baig, A.; Hurrell, E.; Zhukov, A.; Langmead, C. J.; Weir, M.; Marshall, F. H. The properties of thermostabilised G protein-coupled receptors (StaRs) and their use in drug discovery. *Neuropharmacology* **2011**, *60*, 36.

59. Cheng, Y.-C.; Prusoff, W. H. Relationship between the inhibition constant (K_i) and the concentration of inhibitor which causes 50 per cent inhibition (I_{50}) of an enzymatic reaction. *Biochem. Pharmacol*. **1973**, *22*, 3099−3108.

60. Caffrey, M.; Cherezov, V. Crystallizing membrane proteins using lipidic mesophases. *Nat. Protoc*. **2009**, *4*, 706-731.

61. Kabsch, W. XDS. *Acta Crystallog*. **2010**, *D66*, 125-132.

62. Evans, P. R.; Murshudov, G. N. How good are my data and what is the resolution? *Acta Crystallogr*. **2013**, *D69*, 1204-1214.

63. Emsley, P.; Lohkamp, B.; Scott, W. G.; Cowtan, K. Features and development of *Coot*. *Acta Crystallogr*. **2010**, *D66*, 486-501.

64. Afonine, P. V.; Grosse-Kunstleve, R. W.; Echols, N.; Moriarty, N. W.; Mustyakimov, M.; Terwilliger, T. C.; Urzhumtsev, A.; Zwart, P. H.; Adams, P. D. Towards automated crystallographic structure refinement with *phenix.refine*. *Acta Crystallogr*. **2012**, *D68*, 352-367.

65. Chen V. B.; Arendall W. B. 3rd; Headd, J. J.; Keedy, D. A.; Immormino, R. M.; Kapral G. J.; Murray, L. W.; Richardson, J. S.; Richardson, D. C. *MolProbity*: all-atom structure validation for macromolecular crystallography. *Acta Crystallogr*. **2010**, *D66*, 12-21.

66. The PyMOL Molecular Graphics System, Version 1.7.4 Schrödinger, LLC: New York; http://www.schrodinger.com.

GRAPHICAL ABSTRACT

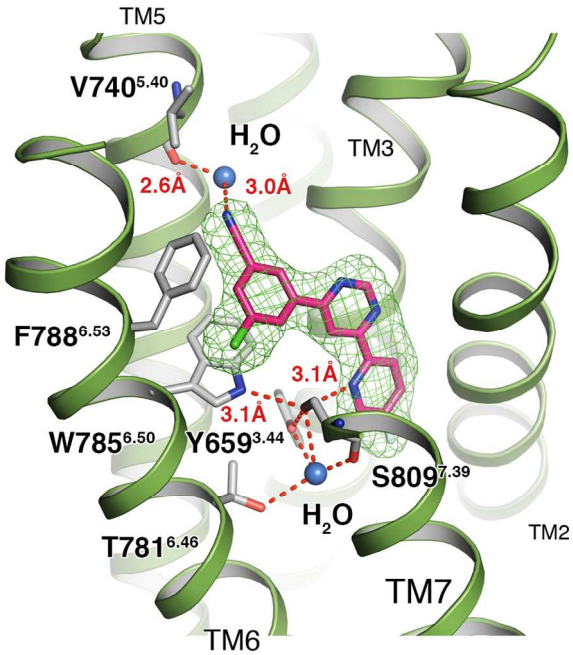

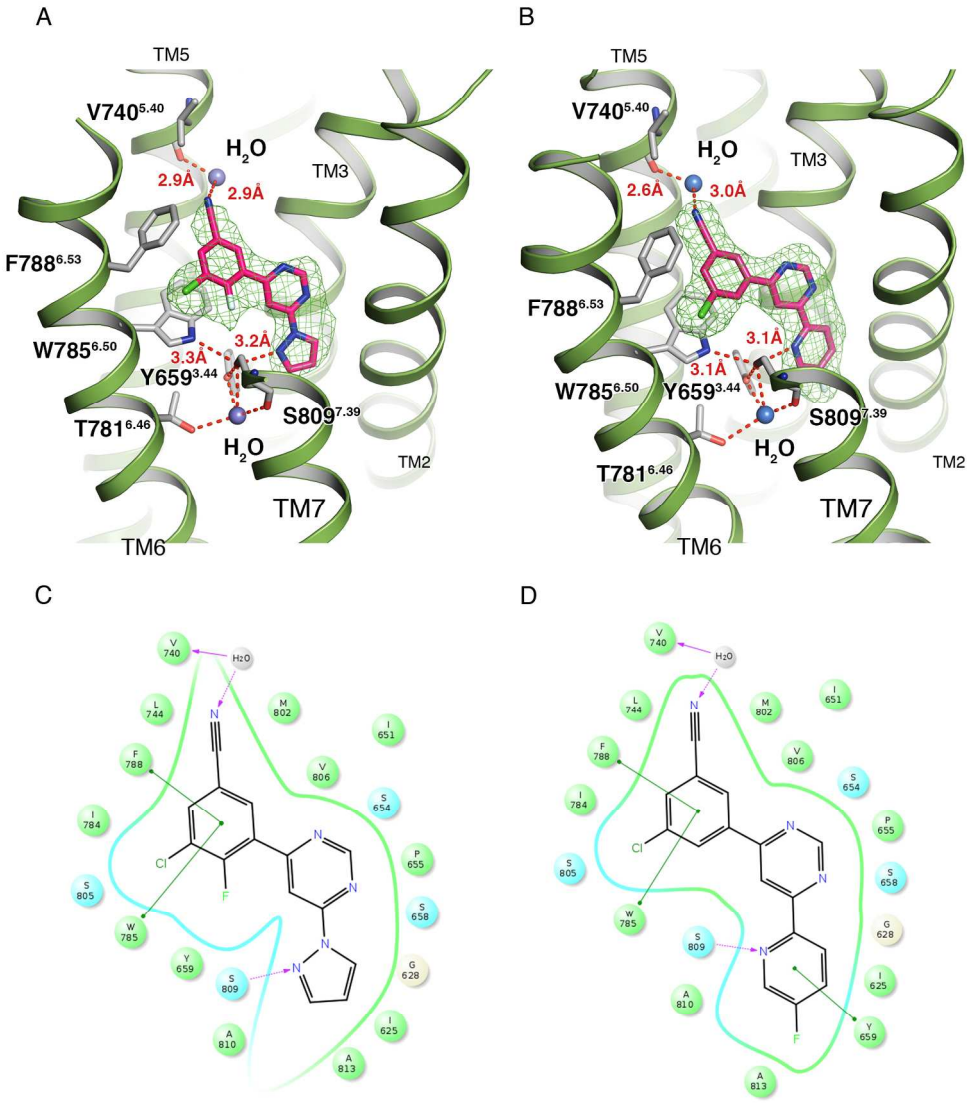

172x192mm (300 x 300 DPI)

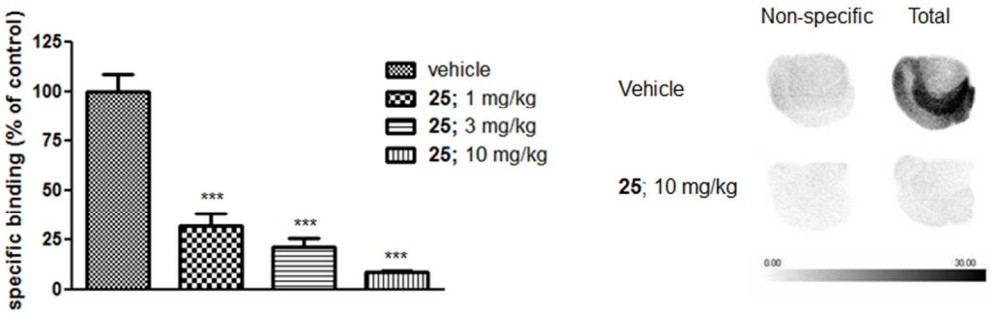

204x64mm (96 x 96 DPI)